Effects of solution conductivity on macropore size dynamics in electroporated lipid vesicle membranes

E. Sabri[1,2], M. Aleksanyan[2,3], C. Brosseau[1,*], and R. Dimova[2]

[1] Univ Brest, CNRS, Lab-STICC, CS 93837, 6 avenue Le Gorgeu, 29238 Brest Cedex 3, France

[2] Max Planck Institute of Colloids and Interfaces, Science Park Golm, 14476 Potsdam, Germany

[3] Institute for Chemistry and Biochemistry, Freie Universität Berlin, Takustraße 3, 14195 Berlin, Germany

* Email: brosseau@univ-brest.fr

1

Abstract

Using fast imaging digital video microscopy, we investigate in detail expansion of micron-sized pores occurring in isolated electroporated giant unilamellar vesicles composed of the phospholipid 1-palmitoyl-2-oleoyl-sn-glycero-3-phosphocholine (POPC). We also develop a computational approach to infer morphological information on the electrodeformed and electropermeabilized vesicles, and test the well-established prediction of Smith, Neu and Krassowska (SNK). The analysis we describe is consistent with the expected outcome of an SNK extension of the electrical force acting on a hydrophilic pore which is induced by the local transmembrane potential. It also provides a new theoretical perspective on how the conductivity ratio of the inside and the outside vesicle solution plays a determinant role in the definition of this electrical force driving pore expansion kinetics.

I. Introduction and motivation

Recent literature has presented significant progress in understanding the possible mechanisms of electropermeabilization (EP) of biological cells and lipid vesicles [1-10]. In these settings, there has been a longstanding debate over the mechanism of pore opening and expansion across cell membranes and/or lipid bilayer. Some authors argue for a rearrangement of the phospholipid bilayers under strong electric field excitation and the formation of aqueous pores. However, their origin, or formation of voltage gated channels, remains a crucial open question. This challenge is further compounded by the role of the outside vesicle environment which eventually impacts significantly the shape of the vesicle, i.e. role of the electrical conductivity ratio Λ of the inside and the outside vesicle solution. In general terms, lipid membranes can be treated as incompressible fluid interfaces and hold significant promise as an arena for investigating multiphysics cell model membranes. Additionally, there does seem to be (at least) a consensus that the pore size and transmembrane potential, V_m, are two critical variables in determining EP dynamics, but little is known about the contribution from each cue individually, see e.g. Refs. [7-8]. Current strategies for visualizing the time-dependent behavior of individual electropores in vesicles rely on detecting the dynamics of solute flow between the internal and external volumes [10], or using optical single-channel recording and fluorescence imaging of bilayers [6].

In light of the above, this work considers a tractable geometric configuration of lipid vesicles for which the ED and EP properties can be studied simultaneously. In this regards, we highlight the importance of computing a membrane related electromechanical quantity, the Maxwell stress tensor (MST), for the multi-physics multiscale simulation of ED and EP. On the experimental side, the electropore growth times are characterized by studying the dynamics of solute flow between the internal and external volumes of giant unilamellar vesicles composed of POPC. We find that the conductivity ratio Λ impacts significantly the rate of change of the size of a macropore occurring in electrodeformed and electropermeabilized vesicles. To explain these differences, we compare the electrical force acting on a transient macropore which is induced by the local transmembrane potential obtained from simulations with experimental data. The quadratic dependence of the electric force expanding the pore with V_m is consistent with an extension of the SNK model as Λ is varied over two orders of magnitude.

II. Background

From the perspective of today's understanding of electropermeabilized lipid vesicle membranes the approach of SNK [9] attempts to predict the expansion of macropores based on the integration of the MST over the internal surface delimiting a pore in the membrane. One question they addressed was how the process of creation and evolution of macropores proceeds during and after the electric pulse excitation. When V_m exceeds the EP threshold, membrane defects begin to occur by thermal fluctuations and energy does redistribute to maintain consistent boundary conditions through a perturbation to the electric field. Once the initial permeabilization of the membrane has occurred, SNK's answer was that the rate of change of pore radius, r, when it is above the minimum pore radius ($r>r^*$), is determined by the force U, so that $\frac{dr}{dt} = \frac{D}{kT}U(r,V_m)$, with

$$U = \sum_{i=1}^{4} U_i = V_m^2 f_{SNK}(r) + \frac{4\beta}{r}\left(\frac{r^*}{r}\right)^4 - 2\pi\gamma + 2\pi\sigma_{eff}r, \quad \text{where} \quad D \quad \text{is} \quad \text{the} \quad \text{diffusion}$$

coefficient of pore radius in the r space [9], k is the Boltzmann constant, T is the absolute

temperature. The first term accounts for the electric force induced by the local value of V_m; the second represents the steric repulsion of lipid heads, the third, for the edge tension opposing the expansion of the circumference of the pore, and the fourth introduces the surface tension of the membrane [9,14]. In the first term, the function $f_{SNK} = F_{max}\dfrac{r+r_1}{r+r_2}$ is obtained by SNK as an approximation of numerical results when Λ is set to 1, F_{max} is the maximal radial force at $V_m = 1$ V, and r_1 and r_2 are two constants [9]. In the other terms, β denotes the steric repulsion energy, r^* is the minimum pore radius, γ is the pore edge tension, and finally, the effective tension of the membrane felt by the pore is $\sigma_{\text{eff}} = 2\sigma' - \dfrac{2\sigma' - \sigma_0}{\left(1 - A_p/A\right)^2}$. Here σ_0 is the surface tension of the membrane without pore, σ' is the energy per unit area of the hydrocarbon-water interface, A is the surface area of the lipid bilayer membrane and the total pore area $A_p = \oiint_S N\pi r^2 \mathrm{d}S$, with S denoting the membrane surface and N is the pore density.

In Fig. 1, the curve for $\Lambda=1$ (SNK) illustrates how the different contributions in U_{SNK} vary with (toroidal) pore radius.
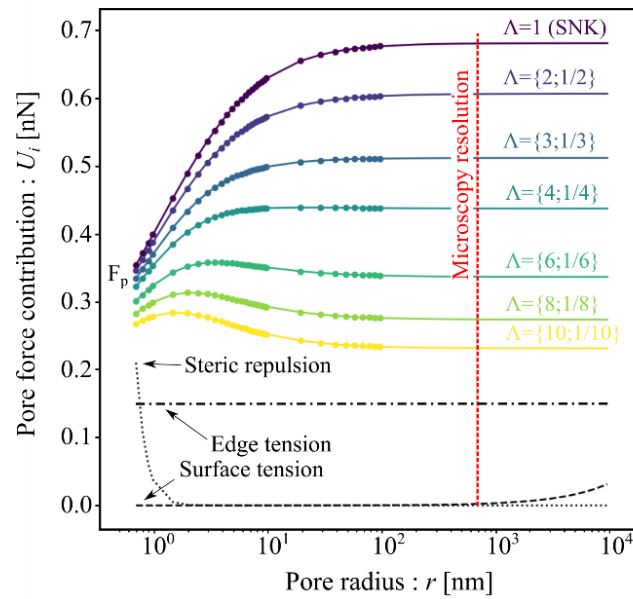
Fig. 1: The predicted change in the four contributions of the force acting on the pore U as a function of pore radius for different values of the electrical conductivity ratio Λ of the inside and the outside vesicle solution. F_p denotes the electromechanical force contribution. Note that for the electric force {i;1/i} means that $f_\Lambda \equiv f_{1/\Lambda}$. Here, the force exerted on a pore by the electric field, for $\Lambda=1$, is computed with $f_{SNK}(r)$ defined in [9], while for $\Lambda>1$, we provide a formula $f_\Lambda(r)$ working for values of Λ. The parameterized analytic function $f_\Lambda(r)$ (solid lines) are shown to match well with the numerical solution (solid symbols). For this calculation we assume $\sigma_{\text{eff}} = 10^{-6}$ N/m and $\gamma = 24$ pN. It is discernible that the electrical component dominates over the other contributions in the entire range of r investigated. The vertical red dotted line represents the limit of our experimental resolution (values of r below this limit are not detected experimentally).

4

The dominant term originates from the electrical force acting on a hydrophilic (conductive) pore which is induced by the local transmembrane potential. This is understood intuitively as the application of V_m changes the free energy of the hydrophilic (conducting) pore such that its free energy is reduced [14-17]. Table I lists the appropriate physical parameters used to get Fig. 1.

Table I: A summary of the parameters used in the computational model for producing the specified figures.

Parameters	Notation	Numerical value
Membrane total thickness	d_m (m)	3.70×10^{-9}
Membrane dielectric thickness	d_{me} (m)	2.71×10^{-9}
Internal medium permittivity	$\varepsilon_0\varepsilon_c$ (Fm^{-1})	7.08×10^{-10}
Internal medium conductivity	λ_{in} (Sm^{-1})	4.4×10^{-4}-6.2×10^{-3}
Membrane permittivity	$\varepsilon_0\varepsilon_m$ (Fm^{-1})	1.77×10^{-11}
Membrane conductivity	λ_m (Sm^{-1})	1×10^{-11}
External medium permittivity	$\varepsilon_0\varepsilon_e$ (Fm^{-1})	7.08×10^{-10}
External medium conductivity	λ_{ext} (Sm^{-1})	4.3×10^{-4}-5.6×10^{-3}
Temperature	T (K)	300
Diffusion coefficient for pore radius	D (m²/s)	5×10^{-14}
Initial surface tension	σ_0 (N/m)	10^{-6}
Steric repulsion energy	β (J)	1.4×10^{-19}
Pore edge tension	γ (N)	43.3×10^{-11}
Energy of hydrocarbon-water interface per unit area	σ' (N/m)	2×10^{-2}
Minimum size of hydrophilic pore at V_m=0 V	r^* (m)	0.51×10^{-9}

For Λ=1, the maximal rate of pore radius change is dictated by the rate at which the cell can be deformed and V_m can be large. It is noteworthy that our model reproduces the outputs of SNK's model for the case Λ=1. However, SNK's model did not include the impact of variations in Λ. Here, we present an extended version of the SNK model (where external medium conductivity and internal medium conductivity are different), and show that the influence of Λ on the expression of the electric force expanding a pore can be well captured if the form of $f_{SNK}(r)$ is changed to $f_\Lambda = F_{max}(r + r_1)\left(\frac{1}{r + r_2} - \frac{\chi}{r + r_3}\right)$, where F_{max}, r_1, r_2, r_3 and χ are constants which depend only on Λ. Table II lists the material properties for cells deduced from consolidated literature data to obtain Fig. 1, and includes details of the numerical method used to compute f_Λ.

Table II: Fit parameters used for the electric force contribution in U_{SNK}, i.e. $F_p = V_m{}^2 F_{max}$ $(r + r_1)\left(\dfrac{1}{r + r_2} - \dfrac{\chi}{r + r_3}\right)$, as a function of the conductivity ratio Λ. Here, the notation $\{i; 1/i\}$ means that $f_\Lambda \equiv f_{1/\Lambda}$.

Λ	F_{max}(nN/V²)	r_1(nm)	r_2(nm)	r_3(nm)	χ
1 (SNK)	0.69	0.23	1.18	0	0
{2;1/2}	1.008	0.242	1.221	1.828	0.399
{3;1/3}	1.599	0.207	1.179	1.544	0.680
{4;1/4}	1.806	0.179	1.079	1.405	0.758
{5;1/5}	1.930	0.157	0.994	1.291	0.803
{6;1/6}	2.186	0.142	0.934	1.183	0.846
{7;1/7}	2.387	0.130	0.880	1.097	0.873
{8;1/8}	2.412	0.121	0.829	1.032	0.887
{9;1/9}	2.356	0.113	0.781	0.980	0.893
{10;1/10}	2.373	0.107	0.744	0.931	0.902

There is an important interesting general lesson here if we consider large pores, i.e. $r \gg 100$ nm (which can also be experimentally detected), we find that $U = V_m{}^2 f_\Lambda(r) - 2\pi\gamma$, by neglecting the contribution of membrane tension which is expected to have a negligible value during the early stages of pore formation and the contribution of the steric repulsion of head groups which is similarly small with respect to its r^{-5} scaling. Thus, the rate of pore expansion during pulse application is given by $\dfrac{dr}{dt} = \dfrac{D}{kT} U \approx \dfrac{D}{kT}(V_m{}^2 f_\Lambda(r) - 2\pi\gamma)$. Due to the large experimental variability of the pore edge tension found for POPC (and $\Lambda = 1$) in the literature, we derive all of our numerical results using an average value of $\gamma = 24$ pN [10,18].

Ultimately our goal is to see how well SNK's model fits with the observed data. This model has several questionable aspects. We note that although the approximations leading to the electric force seem reasonable, it would appear that the details thereof have not been completely disentangled, e.g. the key point to be stressed is that the SNK's model does not consider ED and is therefore unable to predict the impact of Λ on the vesicle deformation. Some experimental work has already highlighted this concern, e.g. [10]. While there has been significant theoretical treatment of planar membranes (e.g. SNK [9]) there has been little study of cell and vesicles membranes with other common shapes (spheroids, ellipsoids) have not been explored beyond a few studies [5,11]. Moreover, the collective nature of SKN's model, i.e. coupling of individual pores through the membrane lipid-water interfacial tension, is still very much unknown, and a wide variety of direct and indirect detection experiments are actively searching for evidence of post-pulse collective membrane resealing kinetics.

Fast digital imaging [10] has offered insight into the deformation and permeabilization of giant unilamellar vesicles subjected to electric pulses of varying strength/duration. The aspect ratio (defined as the ratio of semi-major axis b to semi-minor-axis a of the ellipsoid) of the ellipsoidal deformation for a vesicle (initially spherical) represents a reliable metric for the underlying morphology of the vesicle subjected to electric pulses since it gives a length scale that determines which of the two phenomena (ED and EP) will dominate. Recently [16], there has been an increased emphasis on the role anisotropy may play in the broad set of phenomena described above. When b/a is large at elevated V_m, EP dominates, and maximum membrane deformation coincides with maximum pore aperture. The transmembrane potential for an ellipsoidal membrane can be evaluated [16] as

6

$$V_m(\theta,t) = E_0 \frac{(b^2 - a^2)}{b - \frac{a^2}{\sqrt{b^2 - a^2}} \ln\left(\frac{b + \sqrt{b^2 - a^2}}{a}\right)} \left(\frac{a \cos(\theta)}{a^2 \cos^2(\theta) + b^2 \sin^2(\theta)}\right) (1 - \exp(-(t - t_0)/\tau)), \text{ where } E_0, t, t_0,$$

τ and θ respectively represent the electric field intensity, time, the time of electric pulse onset, the membrane charging time and the angle between membrane surface normal vector and the direction of the field. Using this expression for the transmembrane potential, we can now proceed with comparing theoretically predicted pore expansion rates with experimentally obtained data.

III.   Experimental

Before proceeding with our method for inferring the electrical force on a macropore, we pause to discuss how the experimental results of this study should be interpreted in the light of previous work dealing with the electropermeabilization of giant unilamellar vesicles.

Giant unilamellar vesicles (GUVs) of palmitoyl-2-oleoyl-*sn*-glycero-3-phosphocholine (POPC) (Avanti Polar Lipids, Alabaster, AL) were prepared by using the electroformation method [19], for which 10 μL of a 4 mM of lipid solution prepared in chloroform is spread on the surfaces of a pair of indium tin oxide-coated, conductive glasses (Delta technologies Lt., Germany). Then, the glasses are kept in desiccator for 2 h to remove all traces of the organic solvent. The two glasses are then placed with their conductive sides facing each other and separated by a 2 mm-thick Teflon frame to form a chamber. The chamber is filled with a 200 mM sucrose (Merck, Germany) containing NaCl at concentrations up to 1 mM (Merck, Germany) depending on the desired internal vesicle conductivity. The chamber is then connected to a function generator (Agilent, Germany) and an alternating current (AC) of 1 V with a 10 Hz frequency is applied for 1 hour. After harvesting the vesicle solution from the electroswelling chamber, it is 10-fold diluted in 200 mM of glucose solution (Merck, Germany). The external solution also contained between 0 and 1 mM NaCl to adjust the desired external conductivity. We note that the sugar asymmetry between the interior and the exterior of the vesicle enhances the optical contrast of phase contrast images due to refractive index difference of glucose and sucrose solutions and stabilizes the vesicle position onto the bottom of the electroporation chamber due to the higher density of the sucrose solution in the GUV interior. The osmolarities of sucrose and glucose solutions are measured with a freezing point osmometer Osmomat 3000 (Gonotec GmbH, Germany) and matched to avoid osmotic pressure effects. The conductivities of the sucrose and glucose buffers are measured with SevenEasy Conductivity Device (Schwerzenbach, Switzerland). The results of conductivities are illustrated in Table III.

Table III: Conductivity values for vesicle interior and exterior buffers for the experimental conditions of Figs. 2 and 3.

Conductivity ratio, Λ	Concentration and conductivity of vesicle interior solution	Concentration and conductivity of vesicle exterior solution
0.08	200 mM sucrose, 4.35 ±0.65 μS/cm	200 mM glucose and 1 mM NaCl, 56.68 ± 0.63 μS/cm
0.14	200 mM sucrose, 4.35 ±0.65 μS/cm	200 mM glucose and 0.5 mM NaCl, 32.10 ± 0.08 μS/cm
1	200 mM sucrose, 4.35 ±0.65 μS/cm	200 mM glucose, 4.31 ± 0.35 μS/cm
4.6	200 mM sucrose and 0.5 mM NaCl, 33.69 ± 0.04 μS/cm	200 mM glucose, 4.31 ± 0.35 μS/cm
6.6	200 mM sucrose and 1 mM NaCl, 62.46 ± 2.46 μS/cm	200 mM glucose, 4.31 ± 0.35 μS/cm

The electroporation chamber, purchased from Eppendorf (Eppendorf electrofusion chamber, Hamburg, Germany), consisted of a Teflon frame confined above and below by two glass plates through which observation is possible. A pair of parallel electrode wires (92 μm in radius) is located at the lower glass at a distance of 475 ± 5 μm. The spacing between the electrodes is important for defining the field strength at the location of a selected vesicle above the floor of the chamber. Assuming that the electrodes are perfect cylinders, the distance between the electrodes right at the bottom glass is 674 μm. Because the exact location of the vesicle center of mass above the glass cannot be precisely defined, a nominal gap distance of 500 μm between the electrodes is used, which may induce an error of $\sim$10% for the electric field strength. The chamber is attached to a βtech pulse generator GHT_Bi500 (βtech, l'Union, France), which generates square-wave direct current (DC) pulses. The pulse strength and duration ranges from 8 to 26 V (0.16 ± 0.016 to 0.52 ± 0.052 kV/cm), and 10 to 50 ms, respectively.

An inverted microscope Zeiss Axiovert 200 (Jena, Germany) equipped with a Ph2 20x/0.4 objective is used to monitor GUVs in phase contrast mode. An ultra-high-speed digital camera v2512 (Phantom, Vision Research, New Jersey, USA) is mounted on the microscope and connected to a computer. Image sequences are acquired at 20,000 fps which corresponds to a sampling rate of 50 μs, with resolution of 1.42 pixels/μm. The sample illumination is achieved with a mercury lamp. The onset of pulse application is defined as one frame (50 μs) before visible vesicle deformation occurs. In order to compute the transmembrane potential of the vesicles in their deformed state, the image sequences of a total of 41 vesicles containing a single expanding pore are processed via a contour recognition numerical method [20] which allows us to extract the values of the long and short semi-axis of the vesicles. Pore radii are computed using a lab developed pore edge detection software, PoET based on a numerical method for image processing described in Ref. [17] with a precision of the order of 0.5 μm.

The data are obtained with electropermeabilized giant unilamellar vesicles composed of POPC of radii ranging from 14 to 54 μm filled with 0.2M sucrose solution and immersed in a 0.2M glucose solution to stabilize the stabilize the vesicles osmotically and facilitate pore imaging under phase contrast microscopy. Above a critical V_m close to 1 V for tensionless vesicle membranes [10], the formation of macropores (diameter in the range 0.7-15 μm) with

8

lifetimes of up to a few hundreds of milliseconds is detected. The evolution of the size of a macropore can be individually observed under phase contrast microscopy by tracking the interrupted vesicle contour visualized from difference in refractive indexes between the inner sucrose and external glucose solutions, and computing its radius from a numerical method developed in [17]. As all observed pores are located at the vesicle pole (θ=0) we finally assume that $V_\mathrm{m}=V_\mathrm{m}(\theta=0,t_\mathrm{p})$, where t_p represents the time at which nucleation starts, takes a constant value in the time interval over which $\frac{dr}{dt}$ is measured.

As an illustrative example, Fig. 2 shows the aspect ratio dynamics for the electroporated vesicle corresponding to the same experimental data displayed in Fig. 3, with a nominal applied field strength of 0.24 kV/cm, and $\Lambda = 6.6$. The initial diameter of the vesicle was 23.2 μm and after 50 ms, it was deformed into a prolate spheroid with $b/a = 1.8$. The maximum shape deformation is attained close to the pulse end.
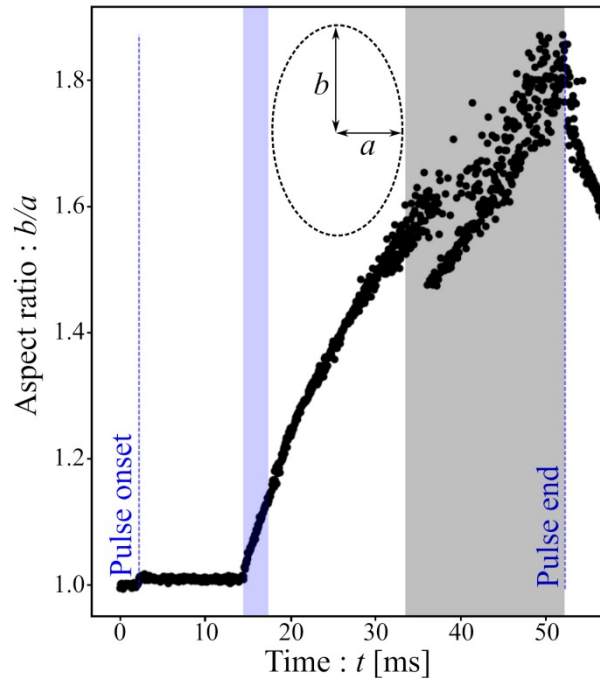
Fig. 2: Time dependence of the aspect ratio of the electrodeformed vesicle during the application of dc electric pulse (0.24 kV/cm, 50 ms). The blue dotted lines indicate the pulse onset and end, respectively. The blue shaded region corresponds to the time interval over which the pore expansion velocity (dr/dt) was considered constant. The grey shaded region represents the time interval over which the pore size was too large for the numerical method we used to accurately interpolate the contour of the deformed vesicle as in the image it was perturbed by the presence of the macropore.

9

IV.   Results and discussion

In the upper top panel of Fig. 3 we show the ED and EP of a POPC vesicle characterized by phase contrast microscopy images. The membrane charging stage starts with the application of the electric pulse to the initially spherical vesicle followed by several electrodeformed states of the ellipsoidal membrane along the direction of the applied field. The macropores are also visualized in the snapshots of the lower top panel using our detection software [17]. The bottom panel of Fig. 3 shows the time evolution of the pore radius following our measurement protocol [17].
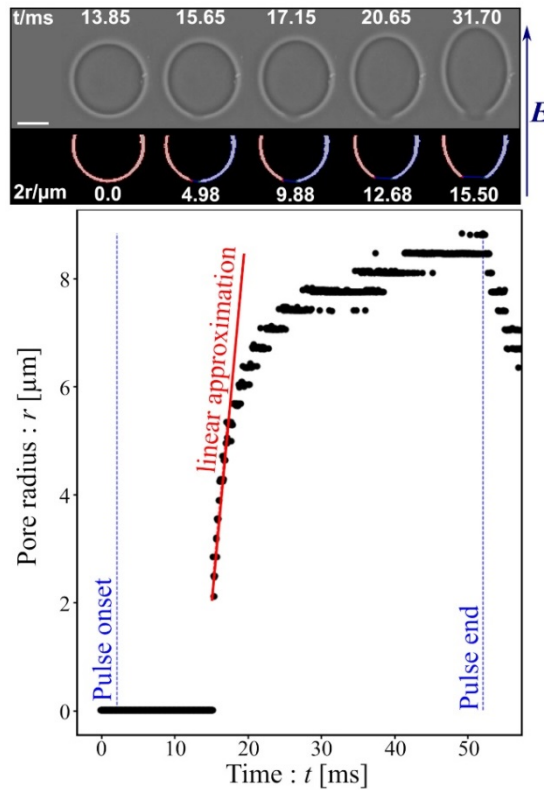
Fig. 3: Pore radius expansion as a function of time during the application of direct current electric pulse (0.24 kV/cm, 50 ms) with Λ=6.6. The top panels show phase contrast microscopy images (upper panel) and software [17] outputs for pore radius computation (lower panel) at different times during pulse application. The scale bar represents 20 μm. The pore diameter, $2r$, and time with respect to the recording onset are indicated in each image. The graph displays the time trace of the pore radius. The blue dotted lines represent the pulse onset and end, respectively. The red line represents the linear approximation of early pore expansion.

The guiding principle of the analysis we propose is this: in order to unravel the impact of conductivity conditions on the rate of expansion of the macropores considered in this study, we focus on the early stages of pore growth where the assumption of a quasi-constant value of V_m is valid. We generated a set of data comprising the pore expansion slopes of all porated GUVs and selected only those for which a single macropore is nucleated in the membrane (Fig. 3). Figure 4 shows the rate of pore expansion as a function of V_m. The dashed lines in Fig. 4 represent the prediction of the extended SNK model for $\frac{dr}{dt}$ at a given value of Λ. The strong correlation between the rate of pore expansion with V_m^2 can be clearly seen from this

10

graph. For all data, the error bars in Fig. 4 represent experimental error associated with estimation of the slope $\frac{dr}{dt}$ and V_m^2 intercept related to the 50 μs time scale of camera sampling.
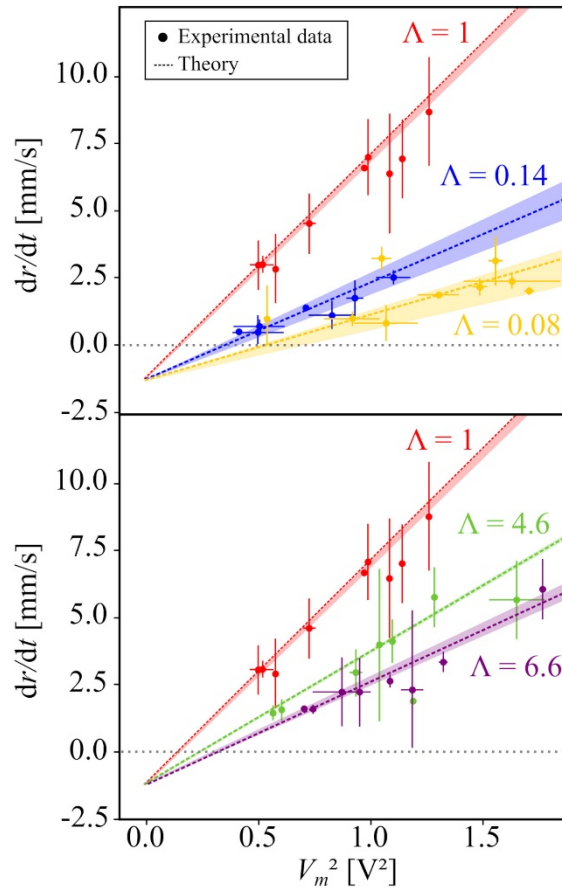
Fig. 4: Dynamics of pore expansion during electric pulse application as a function of the square of the transmembrane potential. Solid symbols show measurements on individual vesicles. For comparison, we also show the extended SNK model (dashed lines), i.e. $\frac{dr}{dt} = \frac{D}{kT}U \approx \frac{D}{kT}\left(V_m^2 f_\Lambda(r) - 2\pi\gamma\right)$, where f_Λ has been introduced to account for differences in conductivity ratio Λ displayed in different colors. The upper panel shows results for $\Lambda < 1$ while the lower panel concerns $\Lambda > 1$. See Table I for the details of the experimental conditions. The shaded regions reflect the error in f_Λ related to the measurement of Λ.

On the simulation side, we use finite element simulations in order to quantify the electromechanical behavior of electropermeabilized lipid vesicle membranes [21-22]. We recently reported on an innovative mechanistic model using the thin-layer approximation (TLA) of cell and vesicle membranes for the multi-physics multiscale simulation of ED to deal with the large differences in dimensions of the different computational domains [11-13]. While in conventional electromechanical scenarios, such cell membrane is treated using a physical thickness, our generic approach is based on an explicit Dirichlet boundary condition (TLA) tailored to tackle the issue of multiscale simulation of ED. If we do not look at the interior of the membrane, but only at its effect on boundary conditions, then it can be replaced by TLA. In the appendix, we outline the procedure employed to compute the MST for computing the electric force expanding a pore and give a detailed description of the definition

of pore conductivity as a function of Λ. For this work we take an electrostatic approach in solving the MST, and we also assume that the membrane can be regarded as an electrically linear, homogeneous isotropic and continuous medium.

The observed broad range of V_m values shown in Fig. 4 can be related to the initial mechanical tension of the membrane, which is expected to lower the EP threshold of the membrane [10,23]. This can be also confirmed by analyzing the linear dependence (Fig. 5) of the relative increase in membrane surface area induced by the application of an electric field, $\alpha_{el} = \dfrac{A - A_i}{A_i}$, on the electrical tension (which is a function of $V_{\mathrm{m}}{}^2$) induced in the membranes, where A and A_i respectively correspond to the surface area of the deformed vesicle and the area of a sphere of equal volume.
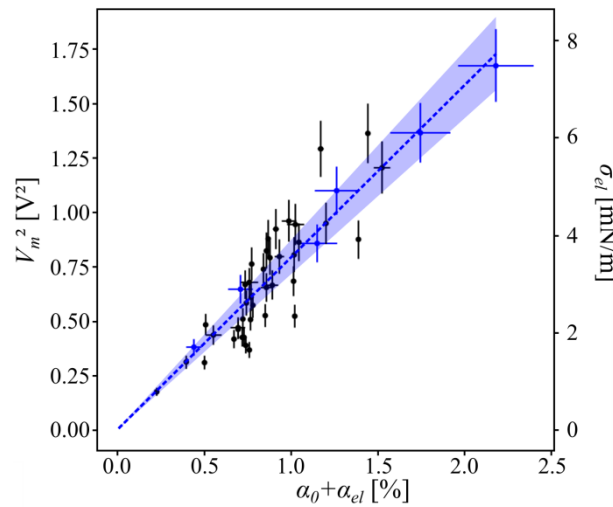
Fig. 5: $V_m{}^2$ and electrical tension σ_{el} induced in the membrane as a function of the total vesicle area increase $\alpha_{tot} = \alpha_{el} + \alpha_0$. The blue symbols and dashed line show the reference experimental data for which $\sigma_0 \approx 0$, while the shaded region shows the associated experimental uncertainty on the value of σ_{el}. Black dots correspond to 40 data points taken from a total of 20 electrodeformed vesicles. The slope of the blue line σ_{el} versus $\alpha_{el} + \alpha_0 \approx \alpha_{el}(\sigma_0 \approx 0)$ yields a value of the membrane stretching modulus of 0.35 ± 0.07 N/m.

Based on the original studies by Helfrich [24], the mechanical deformation and apparent area increase of vesicles subjected to pulse electric fields can be presented as $\alpha_{el} = \dfrac{8\pi\kappa}{kT}\ln\left(\dfrac{\sigma_{el} + \sigma_0}{\sigma_0}\right)$ $+ \dfrac{\sigma_{el}}{K}$, where σ_0 is the initial tension of the vesicle, σ_{el} is the electrical tension induced in the membrane when the vesicle is exposed to the electric field, κ is the membrane bending stiffness (κ is on the order of 30 kT for POPC [25]), and K is the bulk elastic modulus of the membrane (here K is expected to be close to 0.2 N/m [1,25]). It has also been argued by Needham and Hochmuth [23] that if the electrical tension is much larger that the initial tension and if membrane incompressibility is assumed, then the total tension is $\sigma = \sigma_0 + \sigma_{el}$ $= (\alpha_0 + \alpha_{el})K$, where $\sigma_{el} = \varepsilon\varepsilon_0\left(h/2h_e^2\right)V_m^2$ is the electromechanical tension, ε is the permittivity of the membrane, ε_0 the vacuum permittivity, h is the total bilayer thickness, $h\sim$ 3.7 nm, and h_e the dielectric thickness, $h_e\sim$2.7 nm [23]. By contrast with Ref. [23], where the initial tension σ_0 is induced via a pipette aspiration pressure which has for effect to increase the area of an

12

initially unconstrained vesicle by α_0, our vesicle preparation protocol does not permit a full control over the initial area-to-volume ratio of individual vesicles, thus resulting in vesicles with a broad range of initial tensions σ_0 in our experiments. Consequently, a decrease in the initial area-to-volume ratio increases the tension in the membrane, similarly as an isotropic swelling of the vesicle, which can be described by an initial isotropic area increase of α_0. More significantly, the relative increase in area α_{el} induced by the electric field relies on A_i which is a function of the encapsulated volume, and thus of α_0. For a given value of the electrical tension σ_{el}, we argue below that the relative increase in membrane area induced by the electric field can be expressed as $\alpha_{el} \approx \alpha_{el}(\sigma_0 \approx 0) - \alpha_0$, where $\alpha_{el}(\sigma_0 \approx 0)$ accounts for α_{el} in the case an initially tensionless vesicle, i.e. a vesicle that encapsulates a sufficiently small volume of water so that thermal fluctuations would induce a visible flickering of its membrane surface. For that purpose, we consider the dependence of the relative area increase induced by the application of the field $\alpha_{el} = \frac{A - A_i}{A_i}$ on the initial isotropic area increase of α_0. We define α_0 as $\alpha_0 = \frac{A_i - A_0}{A_0}$, where A_i and A_0 respectively represent the initial apparent area of the vesicle and the initial apparent area of the same vesicle in the case of $(\sigma_0 = 0)$. Based on this definition α_{el} can be written as $\alpha_{el} = \frac{A - A_i}{A_i} = \frac{\frac{A}{\alpha_0 + 1} - A_0}{A_0} = \frac{A}{A_0(\alpha_0 + 1)} - 1$. In the case of a negligible initial tension, i.e. $(\sigma_0 = 0)$, we have $\alpha_0 = 0$ where $\alpha_{el}(\sigma_0 = 0) = \frac{A}{A_0} - 1$. Using this relation we get $\alpha_{el} = \frac{\alpha_{el}(\sigma_0 = 0) - \alpha_0}{(\alpha_0 + 1)} \approx \alpha_{el}(\sigma_0 = 0) - \alpha_0$ as $\alpha_0 \ll 1$ in our experiments.

In this context, Fig. 5 was plotted by selecting a vesicle exhibiting a flickering membrane as a reference (blue data) to compute $\alpha_{el}(\sigma_0 \approx 0)$ as a function of σ_{el}. The electrical tension was gradually increased at values above 1 mN/m in order to set our analysis within the boundaries of membrane stretching regime [25] (i.e. corresponding to the case $\sigma_0 \ll \sigma_{el}$), and every data point abscissa was translated by α_0. Then, the data were fitted using the relation $\sigma_{el} = \alpha_{el}(\sigma_0 \approx 0)K$ to compute the stretching modulus K, yielding a value of 0.35 ± 0.07 N/m which is consistent with typical values reported in the literature [10,18]. The values of the initial tensions range from 0.03 mN/m to 4.8 mN/m.

V.   Concluding remarks and perspectives

To summarize, a combination of experimental observations of the dynamic behavior of pores, extended SNK analysis, and simulations by using our TLA-based vesicle model suggests that the conductivity ratio of the inside and the outside vesicle solution has significant and distinctive influence on the rate of change of the macropore size in electropermeabilized lipid vesicles. With the experimental data accessible to us, we have identified the impact of the conductivity ratio on the rate of pore expansion in electropermeabilized membranes. A novelty of our results is given by a precise analytical adaptation of the SNK model allowing us to predict the EP efficiency as a function of conductivity conditions. We also learnt that the basis behind these distinctive behaviors is related to the change in the effective electromechanical behavior of the vesicle with respect to a change in the morphological parameter (i.e. aspect ratio).

Given these observations, it is useful to indicate the senses in which the analysis derived in this study can capture the essence of electrodeformed and electropermeabilized

cells, notably the pore density dynamics in the membrane. Do the electromechanical properties of a cell membrane look like the properties of a stretched lipid bilayer? We first note that intact cell membranes contain many features not found in artificial lipid bilayers. Secondly, phospholipid vesicles are often used as model systems to study the electromechanical properties of ling cells [11-12]. For comparison with biological cells, Λ varies over a range of values 0.1-1 [8,11,16,18]. We expect our analysis will be useful to characterize the electromechanical properties of living cells, and will allow to improve the current disagreement between the current state of the art numerical models and the observed impacts of Λ on electroporation efficiency [7]. A number of points still remain to be investigated, regarding the fundamental issue of the large number of small pores with a random distribution which is more relevant for realistic defective conditions in an electropermeabilized cell [5-6,11]. One important question in this regard is how a SNK generalization can be implemented to deal with the intracellular mechanical changes. This connection needs to be understood in (at least) two different ways. First, there is the problem of understanding strain and stress at interfaces in-between the different phases of the cell [26-28]. And second, there is the solid phase of the cytoplasm (cytoskeleton network and macromolecular crowders) in eukaryotic cells which is known to provide structural support and mechanical stability, and play a fundamental role in controlling the rate at which the cell can be deformed [26-28]. The importance of strain engineering might prove crucial for the design of technologies like vesicle-based biosensors and artificial cells acting as drug delivery carriers. That is a formidable project, extending well beyond what is conventionally considered multiphysics [11-12].

Data availability
The data that support the findings of this study are available from the corresponding author upon reasonable request.

Acknowledgment

References

[1] H. Isambert, "Understanding the electroporation of cells and artificial bilayer membranes", Phys. Rev. Lett. **80**, 3404 (1998); K. Kinosita and T. Y. Tsong, "Formation and resealing of pores of controlled sizes in human erythrocyte membrane", Nature **268**, 438-441 (1977); J. C. Weaver and Y. Chimazdzhev, "Theory of electroporation: a review", Bioelectrochem. Bioenerg. **41**, 135-160 (1996).

[2] K. A. DeBruin and W. Krassowska, "Modeling electroporation in a single cell. I. Effects of field strength and rest potential", Biophys. J. **77**, 1213-1224 (1999); ibidem, "Modeling electroporation in a double cell. II. Effects of ionic concentrations" **77**, 1225-1233 (1999).

[3] E. C. Gianulis, M. Casciola, S. Xiao, O. N. Pakhomova, and A. G. Pakhomov, "Electropermeabilization by uni- or bipolar nanosecond electric pulses: The impact of extracellular conductivity", Bioelectrochem. **119**, 10-19 (2018).

[4] D. Shao, W.-J. Rappel and H. Levine, "Computational model for cell morphodynamics", Phys. Rev. Lett. **105**, 108104 (2010); P. Katira, M. H. Zama, and R. T. Bonnecaze, "How changes in cell mechanical properties induce cancerous behavior", Phys. Rev. Lett. **108**, 028103 (2012); S. Sun, G. Yin, Y. K. Lee, J. T. Y. Wong, and T. Y. Zhang, "Effects of deformability and thermal motion of lipid membrane on electroporation: By molecular dynamics simulations", Biochem. Biophys. Res. Commun. **404**, 684 (2011); Z. Q. Levine and P. T. Vernier, "Life cycle of an electropore: Field-dependent and field-independent steps in pore creation and annihilation", J. Memb. Biol. **226**, 27-36 (2010).

[5] D. Shamoon, J. Dermol-Cerne, L. Rems, M. Rebersek, T. Kotnik, S. Lasquellec, C. Brosseau, and D. Miklavčič, "Assessing the electro-deformation and electro-permeabilization of biological cells using a three dimensional finite element model", Appl. Phys. Lett. **114**, 2019, 063701(1)-063701(5).

[6] J. T. Sengel and M. I. Wallace, "Imaging the dynamics of individual electropores", PNAS **113**, 5281-5286 (2016); J. T. Sengel and M. I. Wallace, "Measuring the potential energy barrier to lipid bilayer electroporation", Philos. Trans. R. Soc. Lond. B Biol. Sci. **372**, 20160227 (2017).

[7] P. Ruzgys, M. Jakutavičiūtė, I. Šatkauskienė, K. Čepurnienė, and S. Šatkauskas, "Effect of electroporation medium conductivity on exogenous molecule transfer to cells *in vitro*", Sci. Rep. **9**, 1436 (2019).

[8] V. Novickij, N. Rembialkowska, G. Staigvila, and J. Kulbacka, "Effects of extracellular medium conductivity on cell response in the context of sub-microsecond range calcium electroporation", Sci. Rep. **10**, 3718 (2020).

[9] K. C. Smith, J. C. Neu and W. Krassowska, "Model of creation and evolution of stable macropores for DNA delivery", Biophys. J. **86**, 2813-2826 (2004); J. C. Neu, K. C. Smith, and W. Krassowska, "Electrical energy required to form large conducting pores", Bioelectrochem. **60**, 107-114 (2003).

[10] M. Yu, R. B. Lira, K. A. Riske, R. Dimova, and H. Lin, "Ellipsoidal Relaxation of Deformed Vesicles", Phys. Rev. Lett. **115**, 128303 (2015); K. A. Riske and R. Dimova, "Electro-deformation and poration of giant vesicles viewed with high temporal resolution", Biophys. J. **88**, 1143-1155 (2005); K. A. Riske and R. Dimova, "Electric pulses induce cylindrical deformations on giant vesicles in salt solutions", Biophys. J. **91**, 1778-1786 (2006); R. B. Lira, F. S. C. Leomil, R. J. Melo, K. A. Riske, and R. Dimova, Advanced Science **8**, 2004068 (2021).

[11] E. Goldberg, C. Suarez, M. Alfonso, J. Marchese, A. Soba, and G. Marshall, "Cell membrane electroporation modeling: A multiphysics approach", Biolectrochem. **124**, 28-39 (2018).

[12] E. Sabri and C. Brosseau, "Thin-layer approximation for the multi-physics and multiscale simulation of cell membrane electrodeformation", Bioelectrochem. **145**, 108055 (2022).

[13] COMSOL Multiphysics version 5.5.

[14] J. Neu and W. Krassowska, "Modeling postshock evolution of large electro-pores", Phys. Rev. E **67** 021915 (2003); W. Krassowska and P. D. Filev, "Modelling electroporation in a single cell", Biophys. J. **92**, 404-417 (2007).

[15] R. W. Glaser, S. L. Leikin, L. V. Chernomordik, V. F. Pastushenko, and A. I. Sokirko, "Reversible electrical breakdown of lipid bilayers: formation and evolution of pores", Biochim. Biophys. Acta **940**, 275–87 (1988).

[16] T. Kotnik, G. Pucihar, and D. Miklavčič, "The cell in the electric field," in *Clinical Aspects of Electroporation*, edited by S. T. Kee, J. Gehl and E. W. Lee (Springer Verlag, 2011), 219-43.

[17] F. S. C. Leomil, M. Zoccoler, R. Dimova, and K. A. Riske, "PoET: automated approach for measuring pore edge tension in giant unilamellar vesicles", Bioinformatics Adv. **1**, vbab037 (2021).

[18] G. B. Melikyan, N. S. Matinyan, and V. B. Arakelian. "The influence of gangliosides on the hydrophilic pore edge line tension and monolayer fusion of lipid membranes", Biochim. Biophys. Acta. **1030**, 11–15 (1990); M. Bloom, E. Evans, and O. G. Mouritsen, "Physical properties of the fluid lipid-bilayer component of cell membranes: a perspective", Q. Rev. Biophys. **24**, 293-397 (1991).

[19] M. I. Angelova and D. S. Dimitrov, "Liposome electroformation", Faraday Discuss. Chem. Soc. **81**, 303–311 (1986); R. Dimova, "Giant vesicles and their use in assays for assessing membrane phase state, curvature, mechanics, and electrical properties", Ann. Rev. Biophys. **48**, 93-119 (2019)

[20] R. S. Gracià, N. Bezlyepkina, R. L. Knorr, R. Lipowsky and R. Dimova, "Effect of cholesterol on the rigidity of saturated and unsaturated membranes: fluctuation and electrodeformation analysis of giant vesicles", Soft Matter, **6**, 1472-1482 (2010).

[21] E. Sabri, S. Lasquellec, and C. Brosseau, "Electromechanical modeling of the transmembrane potential-dependent cell membrane capacitance", Appl. Phys. Lett. **117**, 043701 (2020); E. Sabri and C. Brosseau, "Modelling cell membrane electrodeformation by alternating electric fields", Phys. Rev. E **104**, 034413 (2021).

[22] M. M. Sadik, J. Li, J. W. Shan, D. I. Shreiber, and H. Lin, "Vesicle deformation ad poration under strong dc electric fields", Phys. Rev. E **83**, 066316 (2011).

[23] D. Needham and R. M. Hochmuth, "Electro-mechanical permeabilization of lipid vesicles. Role of membrane tension and compressibility". Biophys. J. **55**, 1001-1009 (1989).

[24] W. Helfrich, "Elastic properties of lipid bilayers-theory and possible experiments", Z. Naturforsch. A **28c**, 693-703 (1973); W. Helfrich, "Blocked lipid exchange in bilayers and its possible influence on shape of vesicles", A **29c**, 510-515 (1974); W. Helfrich, "Steric interaction of fluid membranes in multilayer systems", Z. Naturforsch. A **33**, 305-315 (1978); W. Helfrich and R. M. Servuss, "Undulations, steric interaction and cohesion of fluid membranes", Nuovo Cimento Soc. Ital. Fis D **3**, 137-151 (1984).

[25] R. Dimova, "Recent developments in the field of bending rigidity measurements on membranes", Adv. Coll. Interf. Sci. **208**, 225-234 (2014) ; E. Evans and W. Rawicz, "Entropy-driven tension and bending elasticity in condensed-fluid membranes", Phys. Rev. Lett. **64**, 2094-2097 (1990).

[26] M. Simeonova and J. Gimsa, "The influence of the molecular structure of lipid membranes on the electric field distribution end energy absorption", Bioelectromagnetics **27**, 652-666 (2006); Z. Al-Rekabi and S. Contera, "Multifrequency AFM reveals lipid membrane mechanical properties and the effect of cholesterol in modulating viscoelasticity", Proc. Natl. Acad. Sci. **115**, 2658-2663 (2018); P. Kramar and D. Miklavčič, "Effect of the cholesterol on electroporation of planar lipid bilayer", Bioelectrochem. **144**, 108004 (2022).

[27] E. Moeendarbary, L. Valon, M. Fritzsche, A. R. Harris, D. A. Moulding, A. J. Thrasher, E. Stride, L. Mahadevan, and G. T. Charras, "The cytoplasm of living cells behaves as a poroelastic material", Nature Mat. **12**, 253-261 (2013).

[28] P. Deng, Y.- K. Lee, and T.- Y. Zhang, "A nonlinear electro-mechanobiological coupling model for electropore expansion in cell electroporation", J. Phys. D-Appl. Phys. **47**, 445401 (2012); P. Deng, Y- K. Lee, R. Lin, and T.- Y. Zhang, "Nonlinear electromechanical behavior of cell membrane during electroporation", Appl. Phys. Lett. **101**, 053702 (2012).

Appendix: Computational procedure for assessing the macropore size dynamics in electropermeabilized lipid vesicle membrane

The main point is to review the essential physics for computing the electric force acting on the pore and refer readers to [10] for additional technical details. To represent the components of the lipid vesicle on the same footing, we employ as in our previous work [12] single-phase (isotropic and homogeneous) materials.

Our method follows the same numerical procedure as used by SNK in [9]. Figure A1 shows the 2D axisymmetric configuration comprising four domains: internal fluid, membrane, external fluid and pore, where the size of the system can be scaled in terms of the pore radius r. Dirichlet boundary conditions on top and bottom horizontal boundaries are applied, such as $V(z=0)=0V$ and $V(z=40r)=1V$, to analyze the impact of V_m.
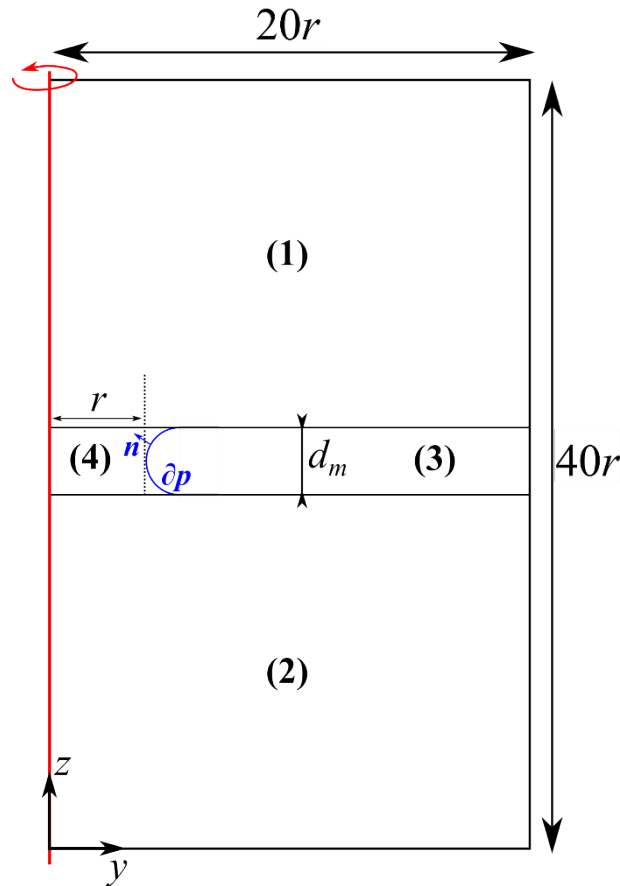
Fig. A1: Sketch (not to scale) of the numerical configuration used to compute the electrical force F_p acting on a pore during pulse application. (1), (2), (3), (4), ∂p and $\boldsymbol{n}$ respectively represent the external fluid, internal fluid, membrane of thickness d_m, the pore of radius r, pore surface and the normal vector to pore surface. The red axis represents the axis of rotational symmetry.

Within each domain, the following set of equations is solved

$$\nabla . \boldsymbol{J} = Q, \tag{A1}$$

18

$$J = \lambda E, \tag{A2}$$

$$E = -\nabla V, \tag{A3}$$

$$T = \varepsilon\varepsilon_0 \left(E \times E - \frac{1}{2}E^2 \right), \tag{A4}$$

where λ, ε, V and Q account respectively for the electrical conductivity, permittivity, electric potential and current density, whereas J, T, and E refer respectively to the surface current density, Maxwell stress tensor, and electric field. Additionally, electric insulation boundary conditions, i.e. $n.J=0$, are applied on the vertical faces of the system while current conservation boundary conditions are applied to all other interfaces. The conductivity of the solution filling the pore is defined as a function of the conductivities of the internal and external solutions, and the vertical coordinate z

$$\lambda_p = \lambda_{ext_p} - \left(\lambda_{ext_p} - \lambda_{in_p} \right)\left(\frac{z + 20r}{h} - \frac{1}{2} \right), \tag{A5}$$

where λ_{ext_p} and λ_{in_p} are respectively defined as

$$\lambda_{ext_p} = \lambda_{ext} - \frac{\lambda_{ext} - \lambda_{in}}{2(1 + 2d_m/(\pi r))}, \tag{A6}$$

$$\lambda_{in_p} = \lambda_{in} + \frac{\lambda_{ext} - \lambda_{in}}{2(1 + 2d_m/(\pi r))}. \tag{A7}$$

A technical point to be made here is that Eq.(A4) allows to compute the MST and the electric force F_p acting on the pore in the membrane plane which is defined as the integral of the normal component of Maxwell stresses over the surface ∂p of the pore (with reference to Fig.A1) as

$$F_p = \iint_{\partial p} n.(T_{(4)} - T_{(3)})n \, dS. \tag{A8}$$

As an aside, we note that the resting potential ($dV/dt=0$) in most polarized cells and vesicles is set to - 70 mV.

From a computational perspective, the numerical analysis was performed via a cluster computer (262 GB RAM, Intel® Xeon® 2.2 GHz (48 CPUs) processor) using the COMSOL simulation package [13]. The mesh is constructed using COMSOL built-in extremely fine element size parameter setting for all domains. Eqs.(S1-S4) are solved using quadratic shape functions within triangular finite elements. Since the size of the system scales with the pore radius r ranging from 0.51 nm to 100 nm, the number of elements discretizing the pore domain is respectively of 577 up to 652, from 5541 up to 1967 elements for the membrane domain, from 94 up to 42 nodes for pore surface, and from 18506 to 35924 for the entire system leading to the resolution of respectively 37315 up to 72205 degrees of freedom which represents to computational times of respectively 21 seconds up to 36 seconds.